

Review

Single Crystal Growth of Synthetic Sulfide- and Phosphide-Based Minerals for Physical Measurements

Paul C. Canfield^{1,2,*}  and Tyler J. Slade¹ ¹ Ames National Laboratory, Iowa State University, Ames, IA 50011, USA² Department of Physics and Astronomy, Iowa State University, Ames, IA 50011, USA

* Correspondence: canfield@ameslab.gov

Abstract: In this work, we review recent advances in the use of high-temperature solution growth that allow for the growth of single crystalline samples of synthetic minerals. We outline how low-melting binary or ternary solutions are attractive solvents for solution growth and provide examples of the growth of bismuthinite (Bi_2S_3), galena (PbS) and parkerite ($\text{Ni}_3\text{Bi}_2\text{S}_2$). We then focus on the Rh-S, Pd-S and Ni-P phase spaces to discuss how the low-melting regions near transition metal-main group eutectic compositions make excellent solvents for crystal growth of several binary and ternary minerals containing both high melting and volatile elements as well as for the discovery of new materials. We end by discussing the growth of synthetic canfieldite (Ag_8SnS_6) and argyrodite (Ag_8GeS_6) from Ag_2S -Sn-S-based solutions.

Keywords: crystal growth; solution growth; synthetic minerals

1. Introduction

Condensed matter research is driven by the discovery of new materials and new ground states. Over the past decades, discoveries of high-temperature superconductivity in cuprates and iron-arsenides [1–3], discoveries of quantum criticality in fragile magnetic systems [4–6], discoveries of previously forbidden symmetries in thermodynamically stable quasicrystals [7–10] and discoveries of high energy density, high-temperature ferromagnets [11] have all created new subfields and motivated the discovery of novel compounds.

Whereas many of the goals or targets of searches for new materials are readily enunciated: better this and bigger that, unexpected behavior, or lower-priced ingredients, the route to such discoveries is less clear and sometimes depends on a combination of keen intuition and pure serendipity, or, stated more technically, a strongly guided or biased random walk through phase space. As in any such endeavor, it is helpful to see what “the competition” is doing, especially if “the competition” has eons more experience. As such, drawing inspiration and taking guidance from nature and mineral systems is a rich and promising starting point for new materials growth and development.

In this article, we outline our use of high-temperature solutions to grow synthetic single crystals of minerals and outline how the mastery of such growths and systems allows us to explore familiar, mineral-based compositional spaces for novel materials and states. We begin with the growth of several binary mineral-based crystals, review the use of binary phase diagrams, and introduce the idea of using solutions based on compositions near eutectic points as (i) promising melts in general and (ii) useful tools for the control and use of volatile elements. To finish, we provide examples of the growth of ternary minerals in the canfieldite (Ag_8SnS_6) and argyrodite (Ag_8GeS_6) phase space. In addition to showing how synthetic single crystalline samples of these minerals can be grown, these results can be used to suggest or outline growth mechanisms or routes that could have taken place in nature over short (hours/days) timelines.



Citation: Canfield, P.C.; Slade, T.J. Single Crystal Growth of Synthetic Sulfide- and Phosphide-Based Minerals for Physical Measurements. *Minerals* **2023**, *13*, 429. <https://doi.org/10.3390/min13030429>

Academic Editors: Huifang Xu and Paul Sylvester

Received: 27 January 2023

Revised: 17 February 2023

Accepted: 9 March 2023

Published: 17 March 2023



Copyright: © 2023 by the authors. Licensee MDPI, Basel, Switzerland. This article is an open access article distributed under the terms and conditions of the Creative Commons Attribution (CC BY) license (<https://creativecommons.org/licenses/by/4.0/>).

2. Discussion

2.1. Single Crystal Growth from High-Temperature Solutions

Using solutions to grow single crystals is an extremely versatile method for inorganic as well as organic compounds [12]. For inorganic compounds, growth from high-temperature solutions (up to 1200 °C or, in some cases, 1500 °C) allows for the growth of oxides, sulphides, borides, intermetallics, etc. and often permits crystallization at considerably lower temperatures than traditional solid-state methods, such as the arc melting and sintering of powders [13–16]. Over the past 30 years, there have been a number of innovations ranging from improvements in how crystals are separated from the remaining solution [17] to innovations in what solutions can be readily used as starting points for growths [15,18–20].

The essence of high-temperature solution growth is cooling a single-phase liquid down to a temperature that lies on the liquidus line, in a binary phase diagram, or liquidus surface, in a ternary phase diagram. Upon intersecting the liquidus, further cooling leads to crystallization and the formation of a two-phase system with the composition of the remaining liquid given by the liquidus line/surface. The binary phase diagrams for Bi-S and Pb-S are shown in Figure 1a,b, respectively. Although elemental sulfur boils below 500 °C, Figure 1a shows that solutions of bismuth and sulfur have greatly reduced vapor pressures. Indeed, as shown by the dotted lines in Figure 1a, a mixture of Bi₆₀S₄₀ can be heated to 1000 °C and still be well below 1 atmosphere of partial pressure. Cooling such a Bi₆₀S₄₀ melt from 1000 to 400 °C over as little as 36 h leads to the formation of well-formed synthetic bismuthinite (Bi₂S₃) crystals (see inset of Figure 1a).

Whereas, in nature, these crystals would be found encased in, or in the vicinity of, elemental Bi, in the lab, we have the luxury of decanting off the excess high-temperature solution once the growth we are interested in is completed. For the case of bismuthinite described above, we would contain the Bi₆₀S₄₀ melt in an Al₂O₃ crucible with an alumina frit and a second, inverted alumina crucible sealed in a silica tube [16,17]. Once the cooling from 1000 to 400 °C is finished, the sealed growth ampule can be removed from the furnace and inverted into a centrifuge so as to decant the excess liquid with the grown crystals staying on the growth side (either due to adhesion to the crucible or the filtering action of the frit). Crucibles of 2, 5 and even 10 mL volumes can be readily used, allowing for single crystals as large as several cubic cm or larger.

In a similar manner, sulfur can be dissolved into Pb, again, with greatly reduced vapor pressures. Synthetic galena (PbS) can be readily grown from a Pb₉₀S₁₀ mixture; heating it to 1000 °C and cooling to 600 °C over as little as 15 h. After decanting off the excess Pb, well-faceted twins (twinned along the crystallographic [111] direction) are revealed (inset of Figure 1b). In both the case of the bismuthinite as well as the case of the galena, larger, and, in some cases, better-formed crystals could be grown by slowing down the nucleation and growth by increasing the cooling times by factors of 2, 4, 8 or 16, depending on the experimental requirements on sample size.

Of course, there is no reason to be limited to two dimensions, as with A. Square in the classic geometric love story, “Flatland” [21], we can consider an additional dimension: ternary (and quaternary) compounds can also readily be grown. For example, single crystals of synthetic parkerite (Ni₃Bi₂S₂) can be grown by adding Ni to a Bi-rich, Bi-S melt. Initial melts ranging from Bi₈₈Ni₆S₆ to Bi₇₀Ni₁₇S₁₃ were cooled from 1050 to 550 °C and yielded crystals of Ni₃Bi₂S₂ [19]. Parkerite is a rare mineral superconductor, albeit with a very low critical temperature of T_c ~ 0.75 K.

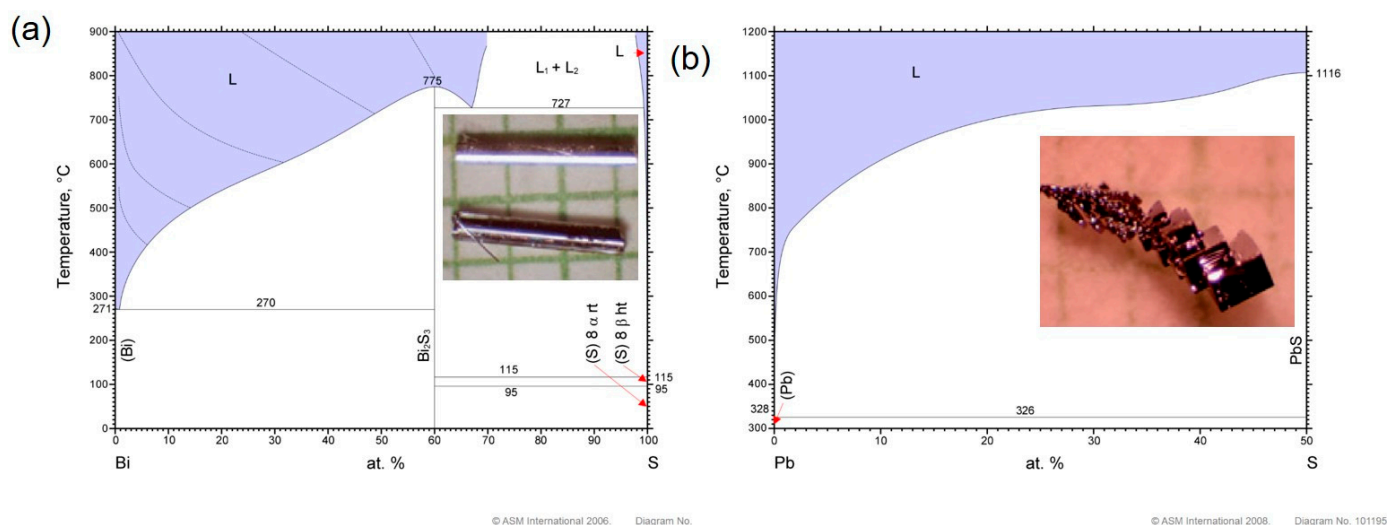


Figure 1. Binary phase diagram of (a) Bi-S (ASM diagram #981133) [22] and (b) Pb-rich side of Pb-S (ASM diagram #101195) [23]. Note: dotted lines in (a) indicate isobars at (from top) 10^5 , 10^3 , 10, 10^{-1} and 10^{-3} Pa. The inset in (a) is a picture of Bi_2S_3 crystals, and the inset in (b) is a picture of PbS crystals. The crystals in each picture are on a mm grid.

2.2. Growth out of Liquids Based on Binary Eutectic Compositions

The growth of bismuthinite and galena were examples of using a low-melting element, Bi or Pb in these examples, as the basis of the “high-temperature solution”. In each case, we simply added some S to the element and could cool the melt back down to near the elemental melting temperature. Whereas this is conceptually simple, it is not the only way to approach the growth of synthetic minerals out of high-temperature melts. In Figure 2, we show three binary phase diagrams of relatively high-melting transition metals with volatile chalcogen or pnictogen elements: Rh-S, Pd-S and Ni-P. The common feature shared by these three binary phase diagrams is a rather deep eutectic close to the transition metal side.

In each case, the eutectic temperature is over 500 °C lower than the melting temperature of the associated metal. Whereas the difficulty in working simultaneously with high melting and volatile elements makes such pairs poorly suited for traditional solid-state synthesis techniques, we have shown over the past years that the low-melting compositions near the eutectic composition can be used as low-vapor-pressure melts that allow access to difficult to grow binary compounds as well as serve as the starting point for ternary melts that can allow for the growth of ternary compounds based on the volatile/refractory pair [19,20].

We can start with the Rh-S binary phase diagram shown in Figure 2a. The liquidus line for miassite ($\text{Rh}_{17}\text{S}_{15}$) is clearly accessible and can be intersected by cooling a $\text{Rh}_{60}\text{S}_{40}$ melt from 1150 to 920 °C over 50 h. After decanting the excess liquid, mm sized, well faceted crystals were found. Temperature dependent electrical resistivity and magnetization measurements show that synthetic miassite has a superconducting critical temperature of 5.3 K. In a similar manner, the Pd-S binary phase diagram (Figure 2b) indicates that synthetic crystals of a Pd-rich variant of braggite (PdS) can be grown as well as Pd_4S . Whereas these Pd-S compounds have been suggested to form from hydrothermal reactions, melting temperatures as low as 650 °C and the fact that these minerals are often reported in nuggets from alluvial deposits with platinum sulfides suggests that natural growth out of Pd-S melts is another strong possibility.

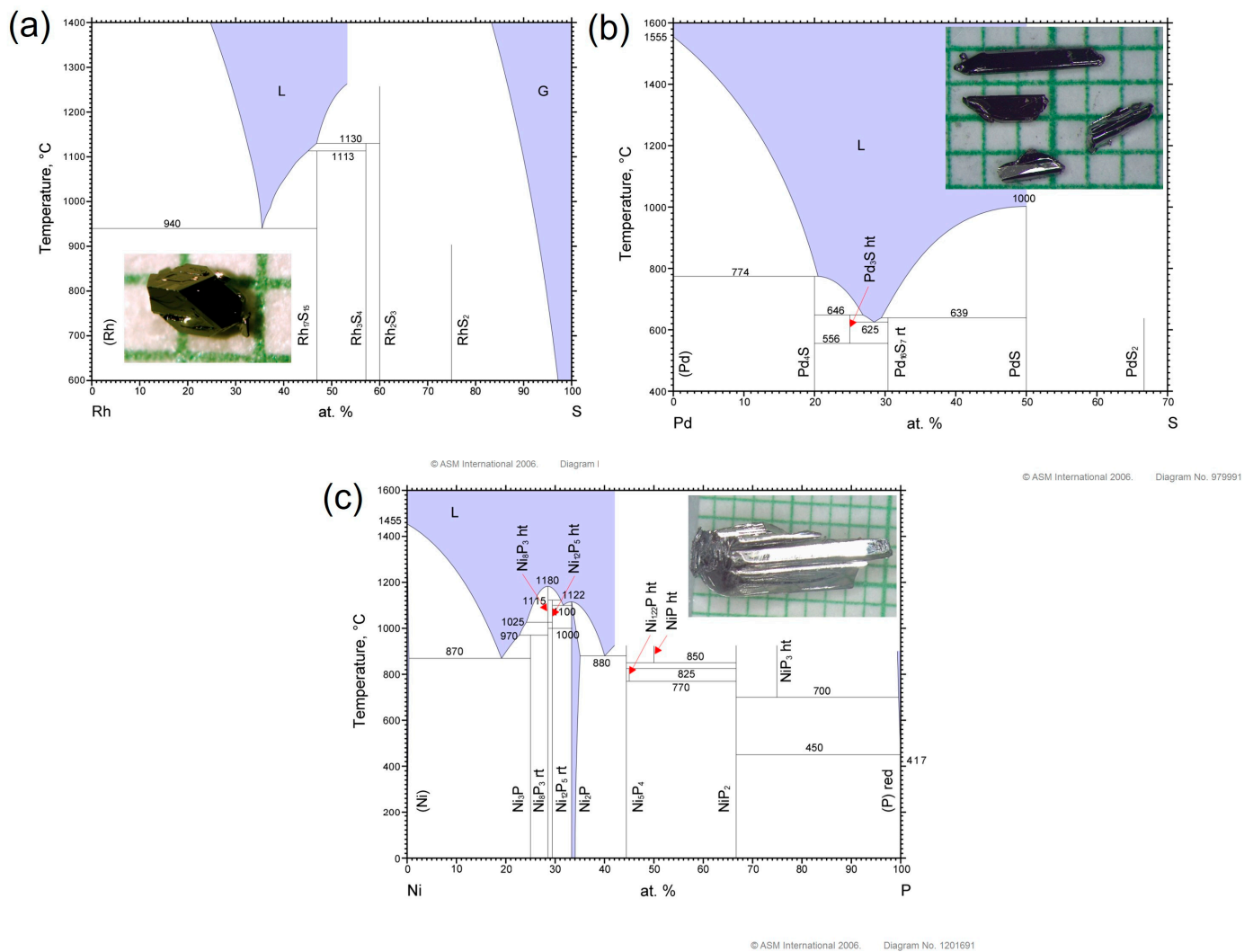


Figure 2. Binary phase diagrams for (a) Rh–S (ASM diagram #980012) [24], (b) Pd–S (ASM diagram #979991) [25] and (c) Ni–P (ASM diagram #1201691) [26]. The insets are pictures of (a) Rh₁₇S₁₅ (miassite), (b) PdS (braggite) and (c) Ni₂P (allabogdanite) on mm grid paper.

Figure 2c presents the Ni–P binary phase diagram. Phosphorous boils at ~300 °C, an even lower boiling temperature than S. As was the case for the transition metal rich Rh–S and Pd–S melts with compositions near the eutectic compositions, Ni–P melts with compositions near Ni₈₁P₁₉ and Ni₆₀P₄₀ have sufficiently low vapor pressures and can be contained in evacuated fused silica tubes for temperatures up to 1200 °C. Compositions near these eutectics allow for the growth of synthetic, Ni-rich Schreibersite (Ni₃P) as well as Ni-rich synthetic allabogdanite (Ni₂P).

Whereas, in some cases, we grow the binary mineral for specific physical studies (miassite to study superconductivity and allabogdanite to study possible non-traditional electrical conductivity), these melts often provide the starting point for more complex growth of ternary compounds. For example, once we mastered use of Rh–S melts, we expanded our phase space to ternary systems based on Rh–S and, in doing so, discovered multiple new Rh–S-based superconductors: Bi₂Rh₃S₂, Bi₂Rh_{3.5}S₂ and Rh₉In₄S₄ [27–29]. In a similar manner, we used compositions near the Pd–S eutectic composition to serve as the solution for the growth of RPd₃S₄ (R = Ce and Eu) compounds for the study of mixed valence behavior [20,30–34].

In this latter case, starting compositions of R₅Pd₅₈S₃₇ were fractionated by first cooling from 1150 to 1050 °C to remove solidified slag as well as binary rare earth sulfides and

then resealing the decanted liquid and cooling from 1075 to 900 °C over 150 h. The resultant, up to cm sized, single crystals were then used for detailed thermodynamic, transport, diffraction, and spectroscopic measurements. Mastery of such low-temperature, eutectic-based melts continues to provide fruitful platforms for discovering new materials. Using essentially the same process outlined above, we recently found that, by adding small quantities of 3d transition metals into melts near the Pt-P and/or Pd-P eutectic compositions, we could grow mm-scale single crystals of the new compounds CrPt₅P and MnPd₅P, each of which are high-temperature ferromagnets with respective Curie temperatures of 454 and 295 K [20,35,36].

2.3. Growth of Synthetic Canfieldite (Ag₈SnS₆) and Argyrodite (Ag₈GeS₆)

Canfieldite, and its neighboring argyrodite, are ternary silver chalcogenide minerals that exhibit rich structural chemistry and favorable thermoelectric properties [37,38]. As canfieldite is often found to occur alongside silver and tin sulfides and salts, the use of Ag₂S (acanthite or argentite) to create a high-temperature solution for crystal growth is strongly suggested. Indeed, both the Ag–S and Sn–S binary phase diagrams have accessible liquid regions for compositions near Ag₂S and compositions between SnS₂ and SnS with eutectic temperatures as low as 740 °C. Perhaps more importantly, studies of parts of the ternary Ag–Sn–S phase diagram indicate the existence of an exposed liquidus surface for the primary formation of Ag₈SnS₆ (Figure 3a).

On the basis of the existing phase diagram data, as well as our experience with S-based growths, we used Ag₂S (Alfa-Aesar, Heysham, UK, 99.5%), S (Alfa-Aesar 99.99%) and Sn (Alfa-Aesar, 99.99%) in a molar ratio 35:38:27, respectively, giving a stoichiometry of Ag₄₁Sn₁₆S₄₃ as the initial composition of our melt. Figure 3b presents the Ag–Sn–S ternary phase diagram and shows the pseudo-binary cut associated with Figure 3a as a red line with the target canfieldite shown as a red dot. Our initial melt composition is shown as the blue dot. After confirming that our Ag₄₁Sn₁₆S₄₃ melt was a single phase liquid at 800 °C, we proceeded with crystal growth by heating the mixture to 800 °C, dwelling for 10 h and then cooling over 200 h to 625 °C [39].

After decanting the excess liquid, large, mirror-faceted, single crystals of Ag₈SnS₆ weighing up to 1 g with dimensions as large as 5–10 mm were recovered (see the inset of Figure 3). While studying our synthetic canfieldite specimens, we discovered a new, low temperature structural phase transition near 120 K, in which the *rt-Pna*2₁ structure transforms to a different *Pmn*2₁ arrangement that is isostructural to the selenide analogues Ag₈SnSe₆ and Ag₈GeSe₆ [39]. This first-order transition has an exceptionally large thermal hysteresis and even allows for the quenching of the room temperature structure to 4 K in a long-lived metastable state.

The rich polymorphism characteristic of the argyrodite family [41] encouraged us to further explore the broader argyrodite structure class by systematically replacing Sn with Ge. We found that Ag₈GeS₆ (argyrodite) and alloyed samples (Ag₈Sn_{1-x}Ge_xS₆) can be prepared in the same manner as outlined for Ag₈SnS₆, substituting elemental Ge (Alfa-Aesar, 99.99%) for Sn using initial compositions of Ag₄₁(Sn_{1-x}Ge_x)₁₆S₄₃ to produce single crystals of Ag₈Sn_{1-x}Ge_xS₆ (x = 0.1, 0.25 and 1).

In the case of pure argyrodite (Ag₈GeS₆), we were able to grow crystals as large as 2 g from our ternary melts (see inset of Figure 3). These large crystals are ideally suited for inelastic neutron experiments to investigate the exceptionally soft phonon spectrum found in argyrodite compounds. Furthermore, we found that the substitution of Sn by Ge rapidly eliminated the low-temperature structure change found in Ag₈SnS₆, which we attribute to the chemical pressure associated with partial replacement of Sn atoms with the smaller Ge, consistent with the smaller volume analogues Ag₈GeS₆ and Ag₈SiS₆ adopting the *Pna*2₁ structure as *rt*-Ag₈SnS₆ [39].

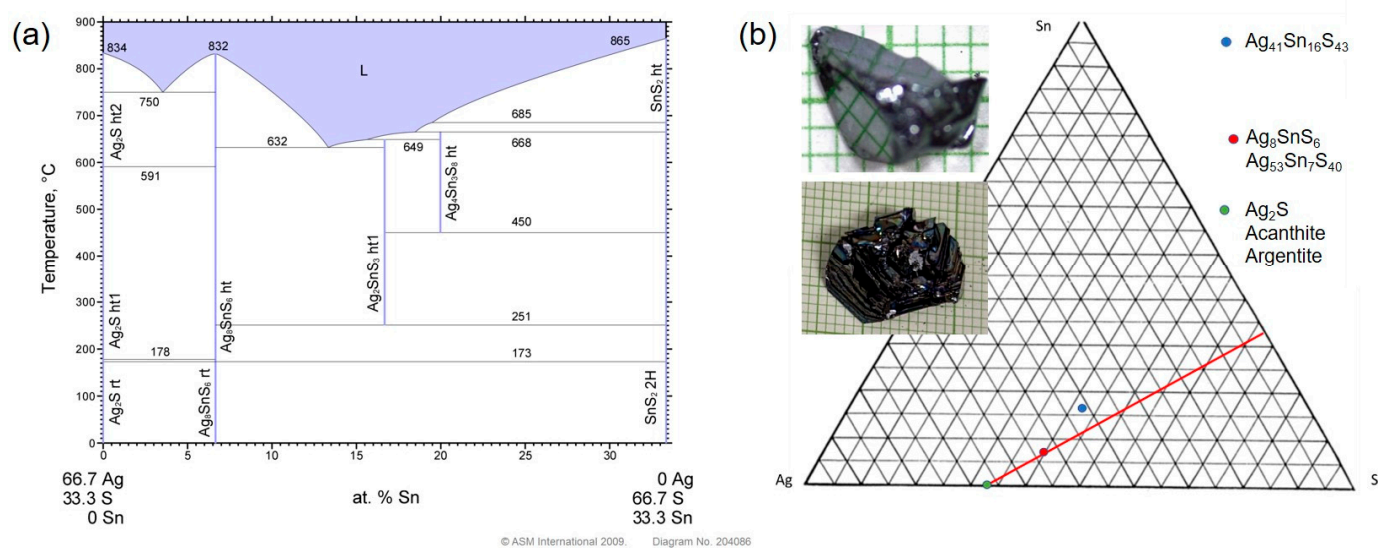


Figure 3. (a) Pseudo binary cut across the Ag-Sn-S ternary phase diagram (ASM diagram #204086) [40]. (b) Ternary Ag-Sn-S phase diagram with the ternary cut shown in (a) as a red line, Canfieldite (Ag_8SnS_6) shown as a red dot, Ag_2S shown as a green dot and our starting melt composition shown as a blue dot. In (b), the upper and lower insets are pictures of a canfieldite (Ag_8SnS_6) and argyrodite (Ag_8GeS_6) crystals on mm grids.

3. Summary

In this brief review, we discussed how synthetic single crystals of many mineral types can be grown out of high-temperature solutions. By using fritted crucibles and decanting off the excess liquid, we can cleanly separate the single crystal samples from the remaining liquid [16,17], thereby, eliminating the problem of separating the specimen from the matrix. Whereas these compounds all can crystallize naturally given suitable conditions and geological time scales, our method allows us to grow high quality single crystals readily out of melts cooled over tens of hours.

Sample sizes are often of the order of the crucible size. The solution-based techniques discussed here should be readily generalizable for the growth of many single crystal mineral (or mineral-based) compounds. Furthermore, the relatively modest melting temperatures exploited by our growths from binary or ternary solutions suggests that the existing mineral samples may have grown from the cooling of complex melts rather than the more typically considered hydrothermal or vapor transport near volcanic vents.

Author Contributions: P.C.C. conceived of and wrote the manuscript. T.J.S. assisted in writing and editing the manuscript. The work was supervised by P.C.C. All authors have read and agreed to the published version of the manuscript.

Funding: This work was supported by the United States Department of Energy, Office of Basic Energy Science, Division of Materials Sciences and Engineering. The research was performed at the Ames National Laboratory. Ames National Laboratory is operated for the U.S. Department of Energy by Iowa State University under Contract No. DE-AC02-07CH11358. T.J.S was supported by the Center for Advancement of Topological Semimetals (CATS), an Energy Frontier Research Center funded by the U.S. Department of Energy Office of Science, Office of Basic Energy Sciences, through Ames National Laboratory under its Contract No. DE-AC02-07CH11358 with Iowa State University.

Data Availability Statement: Data are available from the authors upon request.

Acknowledgments: We would like to acknowledge Frederick Alexander Canfield (1849–1926) for having motivated parts of this research.

Conflicts of Interest: The authors declare no conflict of interest.

References

1. Plakida, N. *High-Temperature Cuprate Superconductors: Experiment, Theory, and Applications*; Springer: Berlin/Heidelberg, Germany, 2010; Volume 166.
2. Proust, C.; Taillefer, L. The Remarkable Underlying Ground States of Cuprate Superconductors. *Annu. Rev. Condens. Matter Phys.* **2019**, *10*, 409–429. [[CrossRef](#)]
3. Stewart, G.R. Superconductivity in iron compounds. *Rev. Mod. Phys.* **2011**, *83*, 1589–1652. [[CrossRef](#)]
4. Stewart, G.R. Heavy-fermion systems. *Rev. Mod. Phys.* **1984**, *56*, 755–787. [[CrossRef](#)]
5. Si, Q.; Steglich, F. Heavy Fermions and Quantum Phase Transitions. *Science* **2010**, *329*, 1161–1166. [[CrossRef](#)] [[PubMed](#)]
6. Canfield, P.C.; Bud'ko, S.L. Preserved entropy and fragile magnetism. *Rep. Prog. Phys.* **2016**, *79*, 084506. [[CrossRef](#)]
7. Charrier, B.; Ouladdiaf, B.; Schmitt, D. Observation of Quasimagnetic Structures in Rare-Earth-Based Icosahedral Quasicrystals. *Phys. Rev. Lett.* **1997**, *78*, 4637–4640. [[CrossRef](#)]
8. Goldman, A.I.; Kong, T.; Kreyssig, A.; Jesche, A.; Ramazanoglu, M.; Dennis, K.W.; Bud'ko, S.L.; Canfield, P.C. A family of binary magnetic icosahedral quasicrystals based on rare earths and cadmium. *Nat. Mater.* **2013**, *12*, 714–718. [[CrossRef](#)]
9. Shechtman, D.; Blech, I.; Gratias, D.; Cahn, J.W. Metallic Phase with Long-Range Orientational Order and No Translational Symmetry. *Phys. Rev. Lett.* **1984**, *53*, 1951–1953. [[CrossRef](#)]
10. Fisher, I.R.; Kramer, M.J.; Wiener, T.A.; Islam, Z.; Ross, A.R.; Lograsso, T.A.; Kracher, A.; Goldman, A.I.; Canfield, P.C. On the growth of icosahedral Al–Pd–Mn quasicrystals from the ternary melt. *Philos. Mag. B* **1999**, *79*, 1673–1684. [[CrossRef](#)]
11. Givord, D.; Li, H.S.; Moreau, J.M. Magnetic properties and crystal structure of Nd₂Fe₁₄B. *Solid State Commun.* **1984**, *50*, 497–499. [[CrossRef](#)]
12. Canfield, P.C. Design, discovery and growth of novel materials. *Philos. Mag.* **2012**, *92*, 2398–2400. [[CrossRef](#)]
13. Scheel, H.J.; Elwell, D. *Crystal Growth from High-Temperature Solutions*; Academic Press Inc.: London, UK, 1975.
14. Pamplin, B.R. *Crystal Growth*; Pergamon Press Ltd.: Oxford, UK, 1975.
15. Kanatzidis, M.G.; Pöttgen, R.; Jeitschko, W. The Metal Flux: A Preparative Tool for the Exploration of Intermetallic Compounds. *Angew. Chem. Int. Ed.* **2005**, *44*, 6996–7023. [[CrossRef](#)] [[PubMed](#)]
16. Canfield, P.C. New materials physics. *Rep. Prog. Phys.* **2020**, *83*, 016501. [[CrossRef](#)] [[PubMed](#)]
17. Canfield, P.C.; Kong, T.; Kaluarachchi, U.S.; Jo, N.H. Use of frit-disc crucibles for routine and exploratory solution growth of single crystalline samples. *Philos. Mag.* **2016**, *96*, 84–92. [[CrossRef](#)]
18. Canfield, P.C.; Fisk, Z. Growth of single crystals from metallic fluxes. *Philos. Mag. B* **1992**, *65*, 1117–1123. [[CrossRef](#)]
19. Lin, X.; Bud'ko, S.L.; Canfield, P.C. Development of viable solutions for the synthesis of sulfur bearing single crystals. *Philos. Mag.* **2012**, *92*, 2436–2447. [[CrossRef](#)]
20. Slade, T.J.; Canfield, P.C. Use of Refractory-Volatile Element Deep Eutectic Regions to Grow Single Crystalline Intermetallic Compounds. *Z. Anorg. Allg. Chem.* **2022**, *648*, e202200145. [[CrossRef](#)]
21. Abbott, E.A. *Flatland: A Romance of Many Dimensions*; Seeley & Co.: London, UK, 1884.
22. Okamoto, H. Bismuth-sulfur phase diagram. In *ASM Alloy Phase Diagrams Database*; Villars, H.O.P., Cenzual, K., Eds.; ASM International: Materials Park, OH, USA, 2016.
23. Okamoto, H. Lead-sulfur phase diagram. In *ASM Alloy Phase Diagrams Database*; Villars, H.O.P., Cenzual, K., Eds.; ASM International: Materials Park, OH, USA, 2016.
24. Okamoto, H. Rhodium-sulfur phase diagram. In *ASM Alloy Phase Diagrams Database*; Villars, H.O.P., Cenzual, K., Eds.; ASM International: Materials Park, OH, USA, 2016.
25. Okamoto, H. Palladium-sulfur phase diagram. In *ASM Alloy Phase Diagrams Database*; Villars, H.O.P., Cenzual, K., Eds.; ASM International: Materials Park, OH, USA, 2016.
26. Okamoto, H. Nickel-phosphorus phase diagram. In *ASM Alloy Phase Diagrams Database*; Villars, H.O.P., Cenzual, K., Eds.; ASM International: Materials Park, OH, USA, 2016.
27. Kaluarachchi, U.S.; Lin, Q.; Xie, W.; Taufour, V.; Bud'ko, S.L.; Miller, G.J.; Canfield, P.C. Superconducting properties of Rh₉In₄S₄ single crystals. *Phys. Rev. B* **2016**, *93*, 094524. [[CrossRef](#)]
28. Herrera, E.; Benito-Llorens, J.; Kaluarachchi, U.S.; Bud'ko, S.L.; Canfield, P.C.; Guillaumon, I.; Suderow, H. Vortex creep at very low temperatures in single crystals of the extreme type-II superconductor Rh₉In₄S₄. *Phys. Rev. B* **2017**, *95*, 134505. [[CrossRef](#)]
29. Kaluarachchi, U.S.; Xie, W.; Lin, Q.; Taufour, V.; Bud'ko, S.L.; Miller, G.J.; Canfield, P.C. Superconductivity versus structural phase transition in the closely related Bi₂Rh_{3.5}S₂ and Bi₂Rh₃S₂. *Phys. Rev. B* **2015**, *91*, 174513. [[CrossRef](#)]
30. Abe, K.; Kitagawa, J.; Takeda, N.; Ishikawa, M. Evidence for Strong Quadrupolar Pair Interactions in Rare-Earth Palladium Bronzes RPd₃S₄. *Phys. Rev. Lett.* **1999**, *83*, 5366–5369. [[CrossRef](#)]
31. Abe, K.; Kitagawa, J.; Takeda, N.; Ishikawa, M. Quadrupolar pair interactions in RPd₃S₄ (R=rare earths). *Phys. B Condens. Matter* **2000**, *281–282*, 597–599. [[CrossRef](#)]
32. Matsuoka, E.; Usui, D.; Sasaki, Y.; Nakao, H.; Shida, H.; Ohoyama, K.; Onodera, H. Simultaneous Occurrence of an Antiferroquadrupolar and a Ferromagnetic Transitions in Rare-Earth Palladium Bronze CePd₃S₄. *J. Phys. Soc. Jpn.* **2008**, *77*, 114706. [[CrossRef](#)]
33. Kitagawa, J.; Takabatake, T.; Matsuoka, E.; Takahashi, F.; Abe, K.; Ishikawa, M. Heterogeneous Mixed-Valence States in RPd₃S₄ (R=Eu and Yb) Viewed from Thermopower, Electrical Resistivity and Specific Heat. *J. Phys. Soc. Jpn.* **2002**, *71*, 1630–1633. [[CrossRef](#)]

34. Ryan, D.H.; Bud'ko, S.L.; Kuthanazhi, B.; Canfield, P.C. Valence and magnetism in EuPd_3S_4 and $(\text{Y, La})_x\text{Eu}_{1-x}\text{Pd}_3\text{S}_4$. *Phys. Rev. B* **2023**, *107*, 014402. [[CrossRef](#)]
35. Slade, T.J.; Mudiyansele, R.S.D.; Furukawa, N.; Smith, T.R.; Schmidt, J.; Wang, L.-L.; Kang, C.-J.; Wei, K.; Shu, Z.; Kong, T.; et al. $\text{Mn}(\text{Pt}_{1-x}\text{Pd}_x)_5\text{P}$: Isovalent Tuning of Mn Sublattice Magnetic Order. *arXiv* **2022**, arXiv:2211.01818. [[CrossRef](#)]
36. Slade, T.J.; Furukawa, N.; Smith, T.R.; Schmidt, J.; Mudiyansele, R.S.D.; Wang, L.-L.; Xie, W.; Bud, S.L.; Canfield, P.C. High Temperature Ferromagnetism in $\text{Cr}_{1+x}\text{Pt}_{5-x}\text{P}$. *Phys. Rev. B* **2023**, *7*, 024410. [[CrossRef](#)]
37. Shen, X.; Xia, Y.; Yang, C.-C.; Zhang, Z.; Li, S.; Tung, Y.-H.; Benton, A.; Zhang, X.; Lu, X.; Wang, G.; et al. High Thermoelectric Performance in Sulfide-Type Argyrodites Compound $\text{Ag}_8\text{Sn}(\text{S}_{1-x}\text{Se}_x)_6$ Enabled by Ultralow Lattice Thermal Conductivity and Extended Cubic Phase Regime. *Adv. Funct. Mater.* **2020**, *30*, 2000526. [[CrossRef](#)]
38. Lin, S.; Li, W.; Pei, Y. Thermally insulative thermoelectric argyrodites. *Mater. Today* **2021**, *48*, 198–213. [[CrossRef](#)]
39. Slade, T.J.; Gvozdet'skyi, V.; Wilde, J.M.; Kreyssig, A.; Gati, E.; Wang, L.-L.; Mudryk, Y.; Ribeiro, R.A.; Pecharsky, V.K.; Zaikina, J.V.; et al. A Low-Temperature Structural Transition in Canfieldite, Ag_8SnS_6 , Single Crystals. *Inorg. Chem.* **2021**, *60*, 19345–19355. [[CrossRef](#)]
40. Okamoto, H. Silver-tin-sulfide phase diagram. In *ASM Alloy Phase Diagrams Database*; Villars, H.O.P., Cenzual, K., Eds.; ASM International: Materials Park, OH, USA, 2016.
41. Kuhs, W.F.; Nitsche, R.; Scheunemann, K. The argyrodites—A new family of tetrahedrally close-packed structures. *Mater. Res. Bull.* **1979**, *14*, 241–248. [[CrossRef](#)]

Disclaimer/Publisher's Note: The statements, opinions and data contained in all publications are solely those of the individual author(s) and contributor(s) and not of MDPI and/or the editor(s). MDPI and/or the editor(s) disclaim responsibility for any injury to people or property resulting from any ideas, methods, instructions or products referred to in the content.